Journal of Alloys and Compounds 815 (2020) 152398

Contents lists available at ScienceDirect

Journal of Alloys and Compounds

journal homepage: http://www.elsevier.com/locate/jalcom

Crystal texture-dependent magnetic and magnetotransport properties of half-metallic Fe_3O_4 films grown on oxidized Si substrates by reactive deposition

V.V. Balashev [a, b, **], K.S. Ermakov [a], A.Yu. Samardak [a], A.V. Ognev [a], A.S. Samardak [a, e, *], S.V. Komogortsev [c, f], M.N. Volochaev [c, d], A.S. Tarasov [c, f], V.V. Korobtsov [a, b]

[a] School of Natural Sciences, Far Eastern Federal University, Vladivostok, Russia
[b] Institute of Automation and Control Processes, FEB RAS, Vladivostok, Russia
[c] Kirensky Institute of Physics, SB RAS, Krasnoyarsk, Russia
[d] Siberian State Aerospace University, Krasnoyarsk, Russia
[e] National Research South Ural State University, Chelyabinsk, Russia
[f] Siberian Federal University, Krasnoyarsk, Russia

ARTICLE INFO

Article history:
Received 6 August 2019
Accepted 21 September 2019
Available online 23 September 2019

Keywords:
Magnetite
Crystal texture
Reactive deposition
Magnetoresistance
Magnetic saturation
FORC

ABSTRACT

Nanocrystalline magnetite (Fe_3O_4) films with various preferred crystallite orientations were grown on oxidized silicon surface by reactive iron deposition in an oxygen atmosphere. Depending on the partial pressure of oxygen (P_{O2}), the evolution of the structural, magnetic, and magnetotransport properties of the grown films was investigated. We found that the growth of films containing only the Fe_3O_4 phase occurs in a certain P_{O2} range, and the magnetite crystallites may have (311) or (110) preferred orientation. It was revealed that films with (311) and (110) textures have a column structure. An increase in the P_{O2} leads to a structure transformation from (311) to (110) texture with larger crystallites. A film with (110) texture showed higher values of saturation magnetization, magnetoresistance and spin polarization. The analysis of approach to magnetic saturation revealed that the local magnetic anisotropy of crystallites in textured films is much higher than the anisotropy of bulk magnetite due to the large surface contribution. The FORC diagram method in combination with the approach to magnetic saturation proved the existence of the exchange coupling between large and small grains. Our results open the reliable route for crystal texture-depending manipulation of functional properties of thin magnetite films for advanced spintronic applications.

1. Introduction

Magnetic and transport properties of magnetite nanoparticles and thin films grown on various substrates have attracted undiverted attention of researchers over the past two decades [1–11]. Magnetite is a promising candidate for spintronics and oxide electronics [12,13] due to the theoretically predicted 100% spin polarization of conduction electrons [14], which is much larger than the experimentally defined values [1,4,15]. In turn, the growth of magnetite films on a silicon substrate is interesting, because there is a possibility of the spin-polarized electrons injection from a ferromagnet into a semiconductor [16,17]. The synthesis of magnetite films is often implemented by methods such as pulse laser deposition (PLD) [18–20] and magnetron sputtering [2,21,22], using an oxygen inlet into the growth chamber during the sputtering of iron or iron oxide from the target. However, it should be noted that the level of the oxygen partial pressure during the growth process may affect the magnetic and electrical properties of the grown Fe_3O_4 films. Thus, the authors of [23] recently showed that this can be attributed to a change in the ratio of ions Fe^{3+}/Fe^{2+} in the inverse spinel lattice of an epitaxial magnetite film. In the case of polycrystalline films, from an analysis of Raman spectroscopy data, it was found that the partial pressure of oxygen affects

* Corresponding author. School of Natural Sciences, Far Eastern Federal University, Vladivostok, Russia.
** Corresponding author. School of Natural Sciences, Far Eastern Federal University, Vladivostok, Russia.
E-mail addresses: balashev@mail.dvo.ru (V.V. Balashev), samardak.as@dvfu.ru (A.S. Samardak).

https://doi.org/10.1016/j.jallcom.2019.152398
0925-8388/

the density of antiphase domain boundaries (APBs) [24], as well as the size of Fe_3O_4 crystallites [2].

The iron oxide films prepared by authors of various works differ in thickness and experimental conditions under which they were grown, which makes it difficult to compare the data. At the same time, it can be said that low oxygen pressure leads to the growth of films with a high iron content [2,25,26], for which magnetic hysteresis loops are characterized by high saturation magnetization (M_s) and low coercive force (H_c). The authors note that a further increase in the oxygen pressure leads to the growth of films in which the M_s and H_c values become comparable for bulk Fe_3O_4. Since, in a certain range of the oxygen pressure, formation of the Fe_3O_4 phase occurs predominantly, a detailed study of properties of the magnetite films as a function of pressure is very interesting. Recently, we have found [27] that, with some pressure variation, a preferred orientation of crystallites appears in the polycrystalline Fe_3O_4 film. This structural change depending on the oxygen pressure was also observed in X-ray spectra [2,28]. Lai et al. [28] showed that ion beam deposition (IBD) of magnetite is accompanied by the appearance of the intense (100) peak on the XRD spectrum with the following attenuation and the amplification of the (311) peak with a subsequent increase in the oxygen pressure. The Fe_3O_4 films deposited by magnetron sputtering [2] had (110), (100) and (111) preferred orientations as a function of the pressure. With the exception of the aforementioned works, there is no complete information about the relationship between the structural, magnetic, and electrical properties of textured Fe_3O_4 films grown at different oxygen pressures. In this work, we have grown magnetite films with different preferred orientations of Fe_3O_4 crystallites using reactive deposition of iron in the oxygen atmosphere. The influence of the crystal structure on the magnetic and magnetotransport properties of the films is studied and discussed in details with help of the first order reversal curve (FORC) diagrams and the approach to magnetization saturation.

2. Experimental details

The magnetite films were grown in an ultrahigh-vacuum setup "Katun" equipped with reflection high-energy electron diffraction system (RHEED, Omicron RH20S) and spectral ellipsometry. Base pressure did not exceed 10^{-10} Torr. Monocrystalline silicon wafers ($0.5 \times 10 \times 20\ mm^3$) of n-type ($7.5\ \Omega\ cm$) with (001) orientation were used as substrates. Before loading the substrates into the vacuum chamber, the cleaning of their surface, as well as the formation of a thin SiO_2 layer (1.5 nm) on it, was carried out in the same way as in Ref. [29]. After loading into the vacuum chamber, samples were preheated at 500 °C for 1 h.

Magnetite films of 75 nm nominal thickness were grown on the SiO_2/Si(001) surface by reactive deposition of Fe in the O_2 atmosphere at the substrate temperature of 300 °C. Iron was deposited at a rate of 2.5 nm/min by thermal evaporation from the Knudsen cell with an alumina crucible (Al_2O_3). Taking into account crystal structure of Fe_3O_4 and Fe, the amount of deposited Fe needed to form a magnetite film with the thickness of 75 nm was approximately half of the film thickness — 37 nm. The films were grown at the following oxygen partial pressures: $1 \cdot 10^{-6}$, $1.5 \cdot 10^{-6}$, $3 \cdot 10^{-6}$ and $7 \cdot 10^{-6}$Torr.

The RHEED patterns were recorded in the process of film deposition at the electron beam glancing angles to the surface ~0.5-1°. After unloading of samples from the vacuum chamber, the structure of films was investigated using transmission electron microscope (TEM HT-7700, Hitachi). The X-ray diffraction (XRD) probing of the magnetite films was carried out on a Bruker D8 Advance X-ray diffractometer (CuKα radiation, 1.54184 Å), in the point-by-point scanning mode. The maximum deviation of the positions of reflections determined using NIST SRM 1976 was less than 0.01° in 2θ. The crystallite size (D_{cr}) was calculated according to the Scherrer equation $D_{cr} = \frac{k\lambda}{\beta}\cos\theta$, where k is the shape factor (0.9 used here), λ is the X-ray wavelength used, β is the full peak broadening (width) at half maximum intensity (FWHM) after subtracting the instrumental line broadening, in radians, and θ is the Bragg diffraction peak angle. This calculation supplements the analysis of TEM images of the thin films.

Studies of the electrical and magnetic properties of the films were carried out at room temperature after unloading samples from the ultrahigh vacuum chamber. Magnetic hysteresis loops and first order reversal curves were obtained by an induction method using a vibrating sample magnetometer (Lake Shore VSM 7410). The resistivity and magnetoresistance measurements of iron oxide films were carried out using a 4-probe method on samples of $4 \times 4\ mm^2$ with help of a measuring module that is a part of VSM. A magnetic field was applied in the film plane (along the line of contact arrangement) in the range of ± 10 kOe.

3. Results and discussion

3.1. Crystal structure characterization

As seen from Fig. 1(a), after deposition of Fe at the low oxygen pressure P_{O2} ~$1 \cdot 10^{-6}$Torr, the RHEED pattern from the surface shows Debye rings and their radii characterize the diffraction from the polycrystalline Fe_3O_4 film. Uniform distribution of the intensity along the rings points to random orientation of the grains in the Fe_3O_4 film. As seen from the TEM image of the film, its thickness is t ~45 nm, not 75 nm as was expected for magnetite structure. The average grain height corresponds to the thickness of this film, and the lateral dimensions are 33 ± 6 nm. The smaller thickness of the iron oxide film can be explained by the incomplete oxidation of Fe, which is directly confirmed by the absence of the more intensive (311) peak of Fe_3O_4, Fig. 1(e). Moreover, there is an indirect confirmation based on the observation of diffusion rings from wustite (FeO) at the initial stage of growth [27]. The observed diffraction rings from magnetite after deposition are associated with the transmission diffraction of electrons in the more oxidized surface layer of the film (grains) consisting of magnetite.

After the deposition of Fe at P_{O2} ~ $1.5 \cdot 10^{-6}$Torr, in the RHEED pattern, instead of continuous rings, arcs were observed, which are characteristic of a Fe_3O_4 film with a texture (Fig. 1(b)). The observed RHEED pattern agrees well with the theoretical one for (100) texture, the axis of which is normal to the surface [29]. It can be seen from the TEM image that the film contains both coarse grains with a height of ~75 nm and lateral size of ~55 ± 11 nm, as well as small grains located at the interface with the SiO_2 layer. If at the initial stage of growth we observed a superposition of arcs and continuous rings in the RHEED pattern, then with an increase in the film thickness, there was a complete transition to broken rings consisting of arcs. It can be assumed that at the initial stage of growth, grains are formed with both random and preferred (100) orientation. The transition to the RHEED pattern, consisting only of arcs from (100) texture, indicates a higher growth rate of grains with (100) orientation. We associate large grains in the TEM image with grains that have a preferred (100) orientation, and small ones, at the interface, with grains with a random orientation. It is interesting to note that in the case of IBD [28] an increase in the pressure/flow of O_2 to a certain value led to an increase in the Fe_3O_4 phase fraction, which was characterized by an intense (400) peak on the XRD spectrum. It is possible that, as in the present work, the Fe_3O_4 film had the (100) texture.

As seen from the TEM image in Fig. 1(c), the Fe_3O_4 film grown at $P_{O2} = 3 \cdot 10^{-6}$ Torr has a columnar structure. The height of the

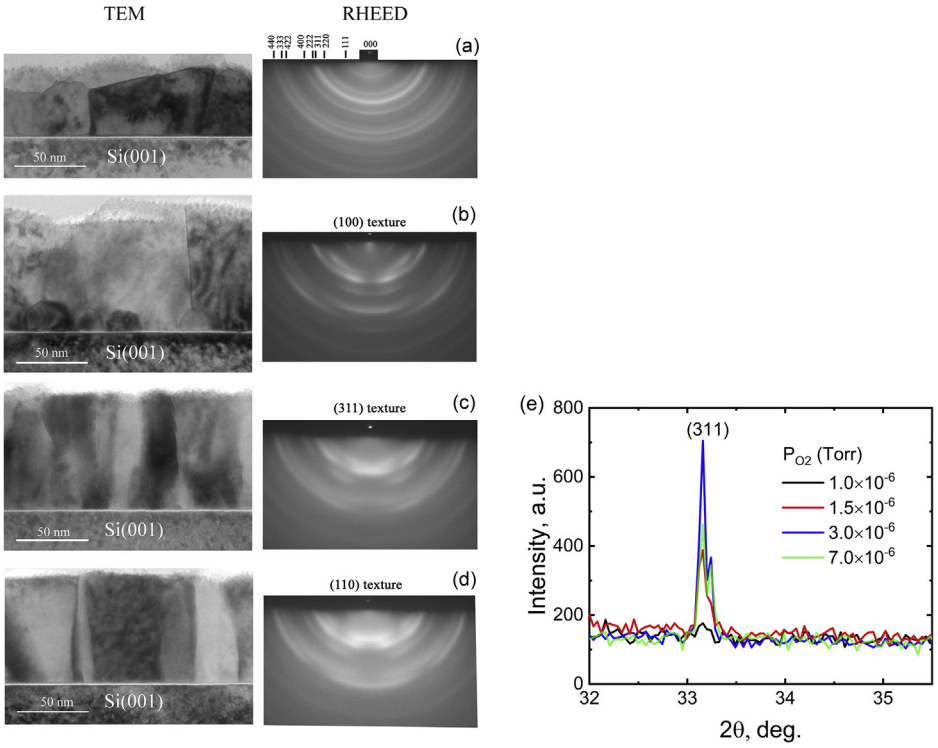

Fig. 1. TEM images and RHEED patterns of Fe_3O_4 films grown at different P_{O2}: (a) $1\cdot10^{-6}$Torr, (b) $1.5\cdot10^{-6}$Torr, (c) $3\cdot10^{-6}$Torr and (d) $7\cdot10^{-6}$Torr. (e) Shortcut XRD spectra for the Fe_3O_4 films grown at different P_{O2}.

largest grains is comparable to the film thickness of 75 nm, while their lateral dimensions (22 ± 3 nm) are approximately three times smaller. Obviously, that these grains have the predominant (311) orientation found from the analysis of the RHEED pattern for this film [27] and confirmed by the XRD study, Fig. 1(e). Film growth at this O_2 pressure occurs according to the competitive mode [30], in which the grain growth in the direction normal to the (311) lattice plane goes faster. The observed transition from (100) to (311) texture was also found in the aforementioned work [28], in which an increase in the oxygen flow led to a complete decay in the intensity of the (400) peak and an increase in the (311) peak.

The magnetite film grown at the higher pressure, $P_{O2} = 7\cdot10^{-6}$ Torr (Fig. 1(d)), also has a columnar structure and consists mainly of large grains. Lateral grain sizes increase by ~2 times compare with the previous film and reach 49 ± 5 nm. According to the analysis of the RHEED pattern [27], this film has the (110) texture. It is assumed that an increase in the O_2 pressure leads to an increase in the diffusion mobility of the adsorbates on {110} faces that have less free energy than the {311} faces. As a result, lateral growth of grains oriented by the corresponding faces parallel to the substrate surface occurs. In this case the film is formed by coalescence [30], rather than the competitive mode of growth. An increase in the lateral size of grains with the O_2 pressure, detected from the TEM data, can serve as a confirmation of this assumption.

As seen in Fig. 1(e), all samples deposited at $P_{O2} \geq 1.5\cdot10^{-6}$ Torr have the (311) peak in the XRD pattern, which is the main indicator of a Fe_3O_4 phase existence. It is worth to note, that in bulk monocrystalline magnetite the (311) peak is situated at $2\theta = 35.423°$. However, deposition of Fe on a Si substrate induces the tensile stresses in thin iron oxide films, which are the main reason for the (311) peak's shift on 2.264° towards smaller angles. This crystal structure transformation increases the interplanar distance in magnetite from 2.534 Å up to 2.702 Å.

Magnetite films grown at low temperatures did not have a texture, and the grain size was several times smaller. In the case of deposition at temperature of ~37 °C using the same deposition method [31], the preferred orientation of the grains of the Fe_3O_4 film was not observed. The author of the work noted that the phase composition of the film fully corresponded to magnetite at the pressure of $P_{O2} = 5\cdot10^{-6}$ Torr. In the case of polycrystalline magnetite films grown at room temperature by magnetron sputtering with thickness of 60 [32] and 70 nm [33], the grains had no preferred orientation as well, and their size was 12–13 nm.

3.2. Magnetic properties characterization

3.2.1. Magnetic hysteresis loop analysis

Fig. 2(a) shows magnetic hysteresis loops measured at 300 K in a magnetic field applied in the plane of films grown at different oxygen pressures. The out-of-plane hysteresis loops (not shown here) have the reduced remnant magnetization (M_r/M_s) close to 0 thereby characterizing the hard magnetization axis for all the samples. This fact indicates that the films have easy plane magnetic anisotropy. It can be seen in (Fig. 2(b)) that the coercive force (H_c) of the film grown at the low oxygen pressure ($1\cdot10^{-6}$Torr) has the smallest value - 160 Oe. With increasing pressure up to $1.5\cdot10^{-6}$Torr, H_c reaches a maximum value of 369 Oe. However, with a subsequent increase in the pressure to $3\cdot10^{-6}$Torr, H_c again decreases to 270 Oe and remains almost unchanged for the film with the (110) texture - 263 Oe, obtained at the higher pressure - $7\cdot10^{-6}$Torr. These values are close to the H_c values for polycrystalline Fe_3O_4 films grown on Si - 300 Oe for t = 80 nm (400 °C) [34], 290 Oe for t = 100 nm (450 °C) [35] and 275 Oe for t = 180 nm (350 °C) [36].

The film grown at the lowest oxygen pressure ($1\cdot10^{-6}$Torr) had the highest saturation magnetization $M_s = 973$ emu/cm^3. The higher M_s value than for bulk magnetite ($M_{bulk} = 471$ emu/cm^3 [37]), as well as the smallest value of the coercive force - 160 Oe, may be associated with the presence of non-oxidized iron in the

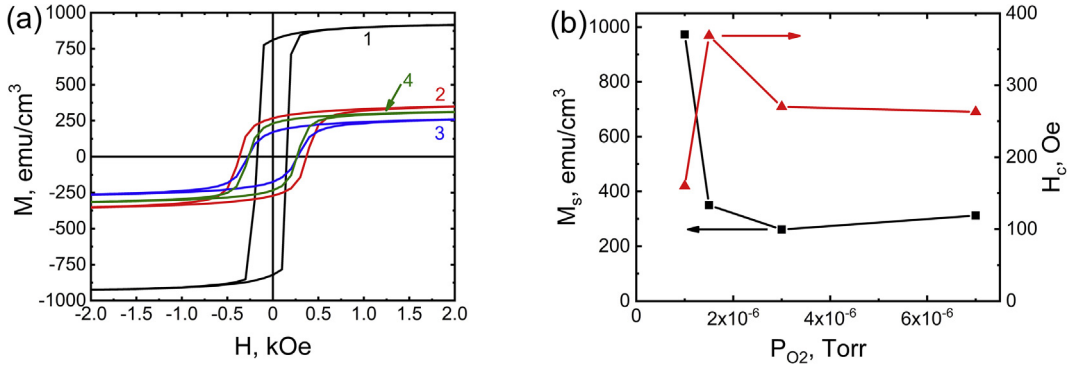

Fig. 2. (a) In-plane magnetic hysteresis loops of the magnetite films grown at P_{O2}: ***1*** - $1 \cdot 10^{-6}$Torr, ***2***–$1.5 \cdot 10^{-6}$Torr, ***3*** - $3 \cdot 10^{-6}$Torr and ***4***–$7 \cdot 10^{-6}$Torr. (b) The dependence of M_s and H_c of the films as a function of the partial pressure of O_2.

film. As mentioned above, this is indirectly confirmed by the small film thickness - ~45 nm, not 75 nm as expected. The value of M_s sharply decreases with the increasing oxygen pressure, Fig. 2(b). Saturation magnetization reaches a minimum value of 261 emu/cm^3 for the film with (311) texture grown at $P_{O2} = 3 \cdot 10^{-6}$Torr. Although the H_c values for films with (110) and (311) textures practically did not differ, the M_s value for films with (110) texture ($P_{O2} = 7 \cdot 10^{-6}$Torr) increased by 51 emu/cm^3 and reached to 312 emu/cm^3. This increase in M_s for a film with (110) texture is associated with an increase in the lateral dimensions of the Fe_3O_4 grains, as found from TEM data analysis. It can be noted that, for a Fe_3O_4 film grown at RT with a thickness of 80 nm and a grain size of ~13 nm, M_s did not exceed 200 emu/cm^3 [33].

The magnetization is determined by the atomic structure and chemical composition of the nearest environment. The decrease in magnetization below the "bulk" value can be explained by defects at the boundaries between crystallites. At the surface of magnetite nanocrystals, the spin-glass state [38,39] is usually realized with the magnetization close to zero. Thus, from saturation magnetization one can estimate the volume fraction of disordered magnetite (in the spin-glass state) at the grain boundaries as:

$$v = 1 - M_s/M_{bulk} \quad (1)$$

The calculated values of ν are shown in Table 1. The defects level of the intercrystalline boundaries is various for different crystal textures. The data in Table 1 enables to observe how the texture and level of structural defects of a magnetite film (associated with grain boundaries) are correlated.

3.2.2. Approach of the initial magnetization curves to magnetic saturation

The approach of the magnetization to saturation for the curves shown in Fig. 3 in the field range from 1 to 10 kOe is described by the following expression [40]:

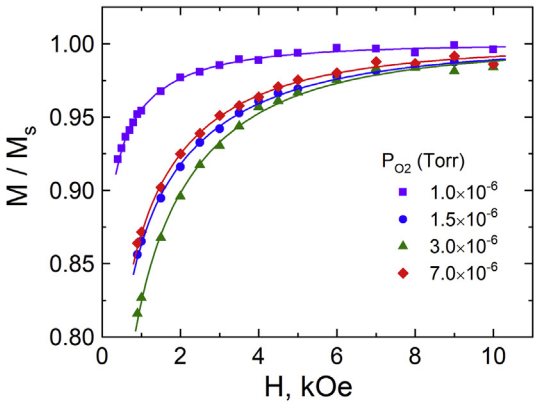

Fig. 3. Approach of the magnetization to saturation of films magnetized in the plane. Solid lines - fitting with equation (2).

$$M(H) = \chi \cdot H + M_s \cdot \left(1 - \frac{(aH_a)^2}{H^{(4-d)/2}\left(H^{d/2} + {H_R}^{d/2}\right)}\right) \quad (2)$$

where $H_R = 2A/(M_s \cdot R_c^2)$, where H_R - the exchange field, A – the exchange stiffness, R_c – the correlation length of the local easy magnetization axis, H_a is the local magnetic anisotropy field of the volume with uniform orientation of the local easy axis of magnetization. It turned out that the best fit is achieved when the dimensionality $d = 3$. The used values of H_R and aH_a are given in Table 1. Parameter $a = \sqrt{1/15}$ for the uniaxial symmetry and $a = \sqrt{2/105}$ for the cubic symmetry of the local magnetic anisotropy for the textureless media. Depending on the sharpness of the texture this coefficient may vary from these values to zero [41]. In addition, for textureless samples, this coefficient would be between the uniaxial and the cubic values [42]. Since we do not have complete quantitative information on the texture and the relative contribution of the uniaxial and cubic components to the local magnetic anisotropy constant, in Table 1 we leave the product aH_a,

Table 1
Parameters of the studied samples.

Sample	P_{O2}, $1 \cdot 10^{-6}$Torr	texture	Grain size, nm	M_s, emu/cm^3	ν	aH_a, kOe	H_R, kOe
1	1	no	33 ± 6	973	-	0.494	2.69
2	1.5	(100)	55 ± 6	350	0.18	1.19	4.44
3	3	(311)	22 ± 3	261	0.37	1.203	3.74
4	7	(110)	49 ± 5	312	0.27	1.037	3.76

which still allows us to judge the level of local magnetic anisotropy.

These data can be interpreted by making preliminary estimates for magnetite. Volumetric magnetite is characterized by cubic magnetic anisotropy with a negative constant of -1.3×10^5 erg/cm^3 [43], the corresponding anisotropy field (540 Oe), saturation magnetization 471 emu/cm^3 and exchange constant 0.7×10^{-6} erg/cm^3. Using this data, the definition of $H_R = 2A/M_s \cdot R_c^2$, and the magnitude of H_R from Table 1, we estimated the size of the localization region of ordering of the local easy axis of magnetization R_c. This estimate gives the length $R_c \sim 8-10$ nm. The magnetic response is the sum of magnetization curves of small (~10 nm without texture) and large (~50 nm) crystallites. Large crystallites are magnetized to saturation in small fields, and small crystallites give that response in the field above 1 kOe, which is fitted by formula (2). Thus, in Table 1 we deal with the parameters of small crystallites. Their local anisotropy is higher than the anisotropy of bulk magnetite, since the surface contribution is already large. The three-dimensional nature of such a response is due to the fact that the small crystallite is exchange-coupled with the large crystallites.

3.2.3. FORC diagram analysis

The method of FORC diagrams [44–46] was used to analyze the magnetic behavior of the magnetite films with different microstructure. Unlike magnetic hysteresis loops, minor reversal curves named FORCs are usually used to analyze reversible and irreversible remagnetization processes and to visualize the interaction (H_u) and switching (H_c) fields distributions. A typical FORC diagram for a magnetic film can be built measuring a family of FORCs at various magnetic fields in the range from −5 to +5 kOe applied parallel and perpendicular to the film plane. First, a sample was saturated in the field $H_s = 5$ kOe and then the field was decreased to H_r. The magnetic moment m was measured in the field H, while it was increasing from H_r to H_s with the step of 50 Oe. The FORC distribution $\rho(H, H_r)$ is defined as the family of mixed derivatives of the second order taken from $m(H, H_r)$:

$$\boldsymbol{\rho}(\boldsymbol{H}, \boldsymbol{H_r}) = -\frac{1}{2}\left[\frac{\partial^2 \boldsymbol{m}(\boldsymbol{H}, \boldsymbol{H_r})}{\partial \boldsymbol{H} \partial \boldsymbol{H_r}}\right] \quad (3)$$

For the better representation of the FORC diagrams, we used a new set of coordinates (H_c, H_u), which were defined as $H_c = \frac{(H-H_r)}{2}$ and $H_u = \frac{(H+H_r)}{2}$.

An effect of the film texture on distributions of H_c and H_u can be seen in Fig. 4. The magnetite film without any texture has very narrow H_c- and H_u-distributions, Fig. 4(a). Texture formation in the films deposited under the higher O_2 pressure leads to the completely different FORC diagrams, Fig. 4(b–d). First of all, the distributions become significantly wider because of the larger variation of grain sizes. Second, the central peaks shifted relatively to H_c-axis to the negative area. Within the variable-variance moving Preisach model this asymmetry is due to that the effective field (H_{eff}) applied to the films can be considered as a sum of the externally applied field (H_{appl}) and the mean field (H_{mean}), which is proportional to the normalized magnetic moment of the sample [47,48]:

$$\vec{H} = \vec{H}_{appl} + \alpha \frac{\vec{m}}{\vec{m}_s}, \quad (4)$$

where α - proportionality constant (moving parameter), m_s – magnetic moment at saturation. As seen in Table 2, the values of H_{mean} are ranging from −30 to −63 Oe. The FORC diagrams have negative regions of $\rho(H_c, H_u)$ which occurrence can be explained as a consequence of mean field interactions in the films [49].

As seen in Table 2, the peak values of H_c defined from FORC diagrams (H_c^{FORC}) corresponds closely to the measured major loop coercive force (H_c^{hyst}), but H_c^{FORC} is a little larger than H_c^{hyst} for all the films. This fact can be attributed to the influence of the mean-field demagnetizing interaction (H_{mean}), which is negative for samples 2, 3 and 4, Table 2. This means that in the textured films H_{mean} works against the external field trying to demagnetize the sample. The main reason for this is the exchange coupling between large and small crystallites, as is discussed in Section 2.2. The FORC diagram for the polycrystalline film (sample 1) has very narrow distributions of H_u and H_c (Fig. 4(a)), which within the classical Preisach model corresponds to the switching of ideal square hysterons [49,50]. The small number of FORCs measured in the switching region between −180 and 180 Oe supports this conclusion. The formation of the crystal texture in the fully oxidized iron films drastically changes the FORC diagrams: the H_u and H_c distributions for samples 2–4 become much wider and the H_c- and H_u-profiles can be described by Gaussian function, Fig. 4(b–d). The variation of the grain size in each film with the texture leads to the grain boundary density variation affecting the switching field distribution much strongly than that in the polycrystalline film.

3.3. Magnetotransport properties

Fig. 5 shows the dependence of the magnetoresistance on the magnitude of the applied external magnetic field (H) for Fe_3O_4 films grown on 1.5-nm-thick SiO_2/Si(001) at different oxygen pressures. The magnetoresistance (MR) was defined as $MR=((\rho(H)-\rho_{max})/\rho_{max}) \times 100\%$, where ρ_{max} is maximum value of resistivity at magnetic field equal to the coercive force - $\rho_{max} = \rho(H_c)$. From Fig. 5 it is clear that for all samples MR is negative and absolute value increases with the applied external field H. The largest values of $MR \sim -2.2$ and -2.5% correspond to Fe_3O_4 films with (311) and (110) textures grown at the pressure of $3 \cdot 10^{-6}$ and $7 \cdot 10^{-6}$ Torr.

An increase in MR for iron oxide films with the increasing O_2 pressure was also observed in Ref. [31]. The maximum MR value there was obtained for a film grown at $5 \cdot 10^{-6}$ Torr, for which, according to Mössbauer spectrum, the phase composition corresponded exclusively to magnetite. The MR value for such a film was ~ −2% at $H = 10$ kOe. The same MR value had a film deposited by magnetron sputtering at RT [32]. As in Ref. [31], smaller MR values for films grown at low pressures ($1 \cdot 10^{-6}$ and $1.5 \cdot 10^{-6}$ Torr) are explained by the presence of the paramagnetic phase FeO, the Debye ring from which we observed by RHEED during the film growth [27]. In contrast to the Fe_3O_4 film deposited at RT in Ref. [31], the films in this work were grown on a hot substrate ($T_{sub} = 300$ °C) and had (311) and (110) textures.

In Ref. [51], the MR value for a 500-nm-thick polycrystalline film with (110) texture grown on a Si substrate was −1.7% at $H = 0.5$ T (5 kOe). This MR value is close to ~ −1.8% for a film with the same texture grown in the present work (curve 4 in Fig. 5), although the grain size in the aforementioned work was 1–2 μm, and in our work it did not exceed 50 nm. In the case of 50-nm-thick films with (111) texture, the MR value was ~1.6% for $H = 10$ kOe [15], which is almost 1% less than for a film with (110) texture grown in this work.

It is assumed that the magnetoresistance is associated with the presence of APBs in the defective places of the Fe_3O_4 film, which have packaging defects in the crystal lattice with a spinel structure. It has been shown that in epitaxial Fe_3O_4 films a change in the density of APBs leads to a change in their conductivity [52] and magnetoresistance [53]. APBs influence (act as a barrier) on electron transport due to the presence of strong antiferromagnetic spin interaction on them. Under the influence of an external magnetic field (H), spin ordering occurs on APBs, as a result of which, the barrier height for electrons tunneling through APBs decreases, and the film conductivity increases [54]. In this case, reducing the

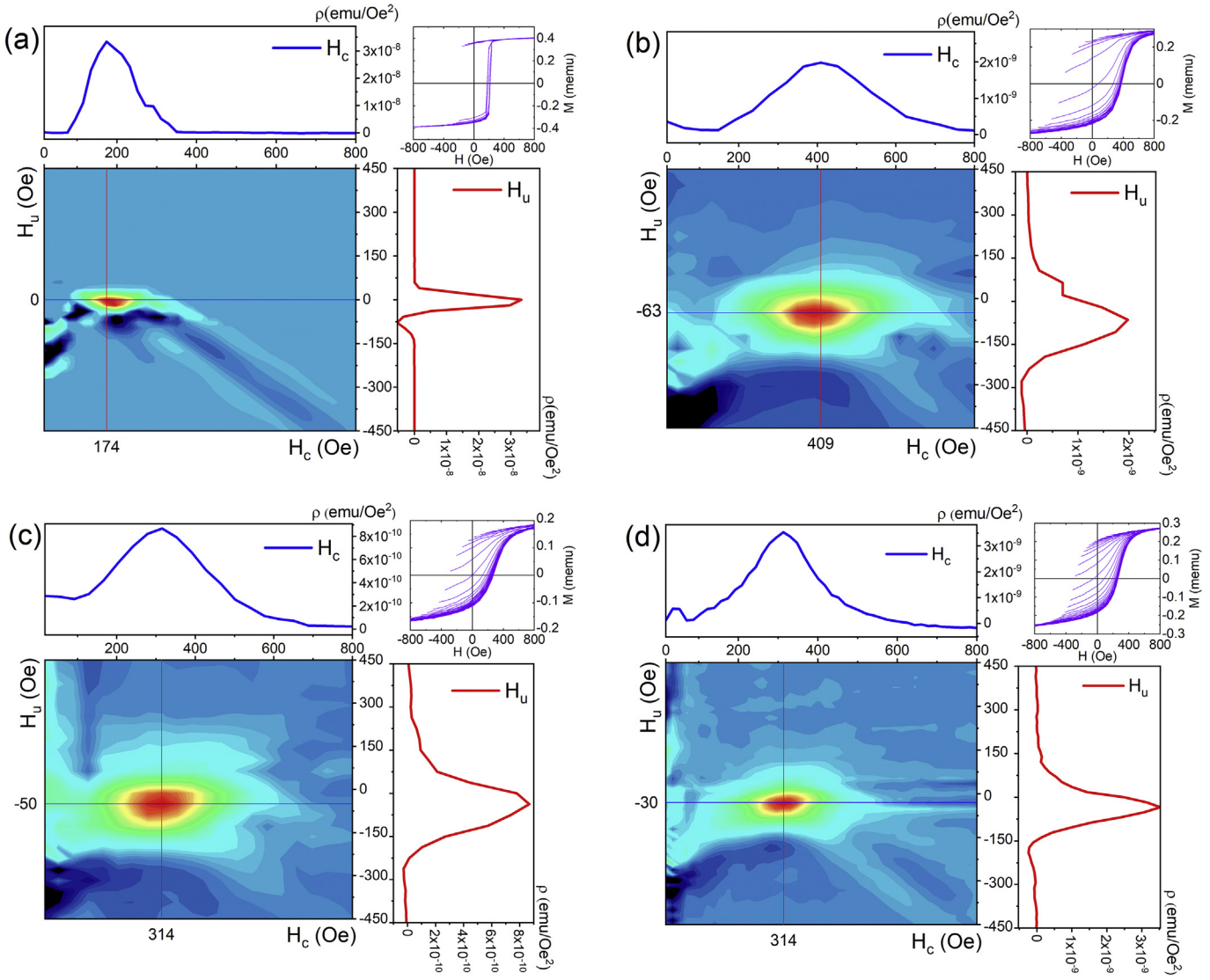

Fig. 4. In-plane FORC diagrams of the magnetite films grown at P_{O2}: ***(a)*** - 1·10^{-6}Torr, ***(b)*** - 1.5·10^{-6}Torr, ***(c)*** - 3·10^{-6}Torr and ***(d)*** - 7·10^{-6}Torr. Each FORC diagram is accompanied with H_c- and H_u-profiles and family of FORCs.

Table 2
Magnetic parameters extracted from hysteresis loops and FORC diagrams.

Sample	H_c^{hyst}, *Oe*	H_c^{FORC}, *Oe*	ΔH_u, *Oe*	H_{mean}, *Oe*
1	168	174	25	0
2	362	409	80	−63
3	270	314	85	−50
4	263	314	48	−30

resistance of the film in the field *H* causes negative *MR* values. In the case of polycrystalline films, grain boundaries and stoichiometry near them should be taken into account. The authors of the works [55,56] noted that magnetoresistance due to spin-dependent scattering within grain boundary (GB) is similar to the case of epitaxial Fe_3O_4 films showing magnetoresistance attributed to scattering at APBs. Since the presence of APBs was observed inside the grains [36], the *MR* value for polycrystalline films should depend on the spin-dependent scattering within both GBs and APBs.

Spin polarization (*P*) of magnetite films depending on texture

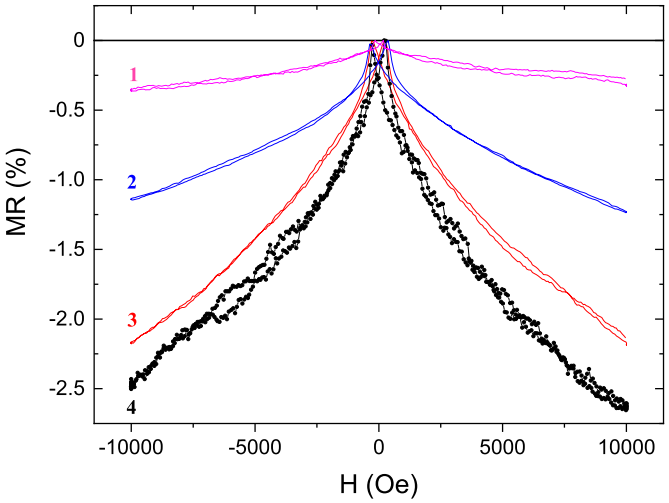

Fig. 5. Magnetoresistance of the magnetite films grown on 1.5-nm-thick SiO_2/Si(001) at various P_{O2}: 1 – 1·10^{-6}Torr, 2 –1.5·10^{-6}Torr, 3 – 3·10^{-6}Torr, 4 – 7·10^{-6}Torr.

was calculated from $P = \sqrt{\frac{MR}{1-MR}}$ [57], where MR is given in absolute values for $H = 10$ kOe, Fig. 5. Magnetite films with (110), (311) and (100) textures have spin polarization 16, 15 and 11%, correspondingly. The film without texture has the minimal value $P = 6\%$. The enhancement of P is possibly due to the decreased density of APBs depending on a texture [15].

The resistivity of films without texture and with (100) texture grown at the low oxygen pressure was 0.045 and 1.45 mOm·cm, that is significantly less than 4 mOm·cm for bulk magnetite [58]. The higher conductivity of the films can be explained by the presence of non-oxidized iron, the existence of which, as mentioned above, was also indicated by the analysis of magnetic hysteresis loops. In contrast, the resistivity values for magnetite films with (311) and (110) textures were higher than 4 mOm·— 0.184 and 0.129 Om·cm. These values are smaller than the values of 0.22 Om·cm [31] and ~0.7 Om·cm [33] for magnetite films without a texture with thickness of 75 and 80 nm grown at low temperature (~300 K). It was noted [31,33] that the value of resistivity strongly depends on the grain size and density of grain boundaries in polycrystalline films. In contrast to the films obtained in this work, the higher resistivity of "low temperature" films with a grain size of ~13 nm [33] can be explained by the higher density of grain boundaries. Larger grains in the case of the film with (110) texture may explain the reduction in resistivity by 30% compared to the film with (311) texture.

4. Conclusions

Using the method of reactive deposition of iron in the oxygen atmosphere, polycrystalline iron oxide films were grown on the surface of a Si(001) substrate with an ultrathin SiO_2 layer. The structural, electrical, and magnetic properties of the films were studied as a function of the oxygen partial pressure. It has been defined that pressure affected not only the phase composition of the films, but also the orientation of the Fe_3O_4 grains formed in them. Starting with the pressure of $3 \cdot 10^{-6}$Torr, the grown film consisted only of magnetite grains with the preferred (311) orientation, and at the higher pressure — with (110) orientation. An analysis of magnetic and electrical data showed that the film with (110) texture has the higher saturation magnetization and the lower resistivity compared to the film having (311) texture. This result is proposed to explain the increase in the size of magnetite grains with the oxygen pressure. It has been found that a magnetite film with (110) texture had the higher magnetoresistance and spin polarization values than films grown at low oxygen pressures. The approach to magnetic saturation in combination with the powerful FORC diagram method proved the existence of the exchange coupling between large and small grains. Our results demonstrate that the textured half-metallic Fe_3O_4 films with controllable properties can be potentially used in complex spintronic devices such as spin injectors, magnetic tunnel junctions, spin filters and spin field effect transistors for future deep integration of spintronics and semiconductor electronics.

Acknowledgments

This work is supported in part by the Russian Ministry of Science and Higher Education under the state tasks (3.5178.2017/8.9 and 3.4956.2017), by Act 211 of the Government of the Russian Federation (contract No. 02.A03.21.0011) and by the Comprehensive Program of Basic Research of the Far Eastern Branch of the Russian Academy of Sciences "Far East" 2018—2020 № 18-3-022 (0226-18-0031).

References

[1] M. Fonin, Y. Dedkov, C. König, G. Güntherodt, U. Rüdiger, J. Mayer, D. Vyalikh, S. Molodtsov, Room temperature spin polarization of epitaxial half-metallic Fe_3O_4(111) and CrO_2(100) films, in: B. Kramer (Ed.), Advances in Solid State Physics, Springer Berlin Heidelberg, Berlin, Heidelberg, 2003, pp. 487—504.
[2] G. Zhang, C. Fan, L. Pan, F. Wang, P. Wu, H. Qiu, Y. Gu, Y. Zhang, Magnetic and transport properties of magnetite thin films, J. Magn. Magn. Mater. 293 (2005) 737—745.
[3] A.M. Bataille, L. Ponson, S. Gota, L. Barbier, D. Bonamy, M. Gautier-Soyer, C. Gatel, E. Snoeck, Characterization of antiphase boundary network in Fe_3O_4(111) epitaxial thin films: effect on anomalous magnetic behavior, Phys. Rev. B 74 (2006) 155438.
[4] M. Fonin, Y.S. Dedkov, R. Pentcheva, U. Rüdiger, G. Güntherodt, Magnetite: a search for the half-metallic state, J. Phys. Condens. Matter 19 (2007) 315217.
[5] R. Prakash, R.J. Choudhary, L.S. Sharath Chandra, N. Lakshmi, D.M. Phase, Electrical and magnetic transport properties of Fe_3O_4 thin films on a GaAs(100) substrate, J. Phys. Condens. Matter 19 (2007) 486212.
[6] S.K. Arora, H. Wu, H. Yao, W.Y. Ching, R.J. Choudhary, I.V. Shvets, O.N. Mryasov, Magnetic properties of ultrathin magnetite films grown by molecular beam epitaxy, Ieee T Magn 44 (2008) 2628—2631.
[7] X. Huang, J. Ding, The structure, magnetic and transport properties of Fe_3O_4 thin films on different substrates by pulsed laser deposition, J. Korean Phys. Soc. 62 (2013) 2228—2232.
[8] M. Imran, A. Akbar, S. Riaz, S. Atiq, S. Naseem, Electronic and structural properties of phase-pure magnetite thin films: effect of preferred orientation, J. Electron. Mater. 47 (2018) 6613—6624.
[9] A.S. Samardak, A.V. Davydenko, A.V. Ognev, Y.S. Jeon, Y.S. Choi, Y.K. Kim, Size-dependent changeover in magnetization reversal mode of self-assembled one-dimensional chains of spherical Fe_3O_4 nanoparticles, Jpn. J. Appl. Phys. 55 (2016) 100303.
[10] P. Prieto, J.E. Prieto, R. Gargallo-Caballero, J.F. Marco, J. de la Figuera, Role of the substrate on the magnetic anisotropy of magnetite thin films grown by ion-assisted deposition, Appl. Surf. Sci. 359 (2015) 742—748.
[11] Y. Liu, R. Wei, W. Ding, X. Wang, W. Song, Z. Sheng, J. Dai, C. Liang, X. Zhu, Y. Sun, Porous Fe_3O_4 thin films by pulsed laser assisted chemical solution deposition at room temperature, Appl. Surf. Sci. 478 (2019) 408—411.
[12] M. Coll, J. Fontcuberta, M. Althammer, M. Bibes, H. Boschker, A. Calleja, G. Cheng, M. Cuoco, R. Dittmann, B. Dkhil, I. El Baggari, M. Fanciulli, I. Fina, E. Fortunato, C. Frontera, S. Fujita, V. Garcia, S.T.B. Goennenwein, C.G. Granqvist, J. Grollier, R. Gross, A. Hagfeldt, G. Herranz, K. Hono, E. Houwman, M. Huijben, A. Kalaboukhov, D.J. Keeble, G. Koster, L.F. Kourkoutis, J. Levy, M. Lira-Cantu, J.L. MacManus-Driscoll, J. Mannhart, R. Martins, S. Menzel, T. Mikolajick, M. Napari, M.D. Nguyen, G. Niklasson, C. Paillard, S. Panigrahi, G. Rijnders, F. Sánchez, P. Sanchis, S. Sanna, D.G. Schlom, U. Schroeder, K.M. Shen, A. Siemon, M. Spreitzer, H. Sukegawa, R. Tamayo, J. van den Brink, N. Pryds, F.M. Granozio, Towards oxide electronics: a roadmap, Appl. Surf. Sci. 482 (2019) 1—93.
[13] T. Banerjee, Oxide Spintronics, Pan Stanford Publishing Pte Ltd, Singapore, 2019.
[14] Z. Zhang, S. Satpathy, Electron states, magnetism, and the Verwey transition in magnetite, Phys. Rev. B 44 (1991) 13319—13331.
[15] E. Liu, Y. Yin, L. Sun, Y. Zhai, J. Du, F. Xu, H. Zhai, Increasing spin polarization in Fe_3O_4 films by engineering antiphase boundary densities, Appl. Phys. Lett. 110 (2017) 142402.
[16] B.T. Jonker, Progress toward electrical injection of spin-polarized electrons into semiconductors, Proc. IEEE 91 (2003) 727—740.
[17] G. Schmidt, Concepts for spin injection into semiconductors—a review, J. Phys. D Appl. Phys. 38 (2005) R107—R122.
[18] M. Bohra, N. Venkataramani, S. Prasad, N. Kumar, D.S. Misra, S.C. Sahoo, R. Krishnan, Study of pulsed laser deposited magnetite thin film, J. Magn. Magn. Mater. 310 (2007) 2242—2244.
[19] J.-G. Yun, Y.-M. Lee, W.-J. Lee, C.-S. Kim, S.-G. Yoon, Selective growth of pure magnetite thin films and/or nanowires grown in situ at a low temperature by pulsed laser deposition, J. Mater. Chem. C 1 (2013) 1977—1982.
[20] S.P. Sena, R.A. Lindley, H.J. Blythe, C. Sauer, M. Al-Kafarji, G.A. Gehring, Investigation of magnetite thin films produced by pulsed laser deposition, J. Magn. Magn. Mater. 176 (1997) 111—126.
[21] E. Aubry, T. Liu, A. Dekens, F. Perry, S. Mangin, T. Hauet, A. Billard, Synthesis of iron oxide films by reactive magnetron sputtering assisted by plasma emission monitoring, Mater. Chem. Phys. 223 (2019) 360—365.
[22] H. Yanagihara, M. Myoka, D. Isaka, T. Niizeki, K. Mibu, E. Kita, Selective growth of Fe_3O_4 and γ-Fe_2O_3 films with reactive magnetron sputtering, J. Phys. D Appl. Phys. 46 (2013) 175004.
[23] J. Zhang, W. Liu, M. Zhang, X. Zhang, W. Niu, M. Gao, X. Wang, J. Du, R. Zhang, Y. Xu, Oxygen pressure-tuned epitaxy and magnetic properties of magnetite thin films, J. Magn. Magn. Mater. 432 (2017) 472—476.
[24] S.K. Singh, S. Husain, A. Kumar, S. Chaudhary, Effect of oxygen partial pressure on the density of antiphase boundaries in Fe_3O_4 thin films on Si(100), J. Magn. Magn. Mater. 448 (2018) 303—309.
[25] C. Schönenberger, S.F. Alvarado, C. Ortiz, Scanning tunneling microscopy as a tool to study surface roughness of sputtered thin films, J. Appl. Phys. 66 (1989) 4258—4261.
[26] Y.K. Kim, M. Oliveria, Magnetic properties of reactively sputtered $Fe_{1-x}O$ and

Fe_3O_4 thin films, J. Appl. Phys. 75 (1994) 431–437.
[27] V.V. Balashev, V.A. Vikulov, T.A. Pisarenko, V.V. Korobtsov, Effect of oxygen pressure on the texture of a magnetite film grown by reactive deposition on a SiO_2/Si(001) surface, Phys. Solid State 57 (2015) 2532–2536.
[28] C.-H. Lai, P.-H. Huang, Y.-J. Wang, R.T. Huang, Room-temperature growth of epitaxial Fe_3O_4 films by ion beam deposition, J. Appl. Phys. 95 (2004) 7222–7224.
[29] V.V. Balashev, V.V. Korobtsov, T.A. Pisarenko, L.A. Chebotkevich, Growth of Fe_3O_4 films on the Si(111) surface covered by a thin SiO_2 layer, Tech. Phys. 56 (2011) 1501.
[30] P.B. Barna, M.S. Adamik, Growth mechanisms of polycrystalline thin films, in: Science and Technology of Thin Films, WORLD SCIENTIFIC, 1995, pp. 1–28.
[31] T. Furubayashi, Magnetoresistance of magnetite films prepared by reactive evaporation, J. Appl. Phys. 93 (2003) 8026–8028.
[32] W.B. Mi, H. Liu, Z.Q. Li, P. Wu, E.Y. Jiang, H.L. Bai, Evolution of structure, magnetic and transport properties of sputtered films from Fe to Fe_3O_4, J. Phys. D Appl. Phys. 39 (2006) 5109–5115.
[33] H. Liu, E.Y. Jiang, H.L. Bai, R.K. Zheng, X.X. Zhang, Thickness dependence of magnetic and magneto-transport properties of polycrystalline Fe_3O_4 films prepared by reactive sputtering at room temperature, J. Phys. D Appl. Phys. 36 (2003) 2950–2953.
[34] C. Boothman, A.M. Sánchez, S. van Dijken, Structural, magnetic, and transport properties of Fe_3O_4/Si(111) and Fe_3O_4/Si(001), J. Appl. Phys. 101 (2007) 123903.
[35] R.J. Kennedy, P.A. Stampe, Fe3O4 films grown by laser ablation on mica with and without MgO buffer layers, J. Magn. Magn. Mater. 195 (1999) 284–290.
[36] J. Tang, K.-Y. Wang, W. Zhou, Magnetic properties of nanocrystalline Fe_3O_4 films, J. Appl. Phys. 89 (2001) 7690–7692.
[37] Magnetic and other properties of oxides and related compounds - Part B, in: K.-H. Hellwege, A.M. Hellwege (Eds.), Landolt-Börnstein - Group III Condensed Matter, Springer-Verlag, Berlin, 1970.
[38] R.H. Kodama, Magnetic nanoparticles, J. Magn. Magn. Mater. 200 (1999) 359–372.
[39] A.P. Safronov, I.V. Beketov, S.V. Komogortsev, G.V. Kurlyandskaya, A.I. Medvedev, D.V. Leiman, A. Larrañaga, S.M. Bhagat, Spherical magnetic nanoparticles fabricated by laser target evaporation, AIP Adv. 3 (2013), 052135.
[40] S.V. Komogortsev, R.S. Iskhakov, Law of approach to magnetic saturation in nanocrystalline and amorphous ferromagnets with improved transition behavior between power-law regimes, J. Magn. Magn. Mater. 440 (2017) 213–216.
[41] R.S. Iskhakov, S.V. Komogortsev, A.D. Balaev, L.A. Chekanova, Dimensionality of a system of exchange-coupled grains and magnetic properties of nanocrystalline and amorphous ferromagnets, J. Exp. Theor. Phys. Lett. 72 (2000) 304–307.
[42] S.V. Komogortsev, S.I. Smirnov, N.A. Momot, R.S. Iskhakov, Technique for determination the energy of uniaxial and cubic magnetic anisotropy in magnetic nanoparticles from experimental magnetization curve, J. Sib. Fed. Unvi. Math. Phys. 3 (2010) 515–520.
[43] J.M.D. Coey, Magnetism and Magnetic Materials, Cambridge University Press, Cambridge, 2010.
[44] I. Mayergoyz, Mathematical models of hysteresis, Ieee T Magn 22 (1986) 603–608.
[45] C.-I. Dobrotă, A. Stancu, What does a first-order reversal curve diagram really mean? A study case: array of ferromagnetic nanowires, J. Appl. Phys. 113 (2013), 043928.
[46] Y. Cao, K. Xu, W. Jiang, T. Droubay, P. Ramuhalli, D. Edwards, B.R. Johnson, J. McCloy, Hysteresis in single and polycrystalline iron thin films: major and minor loops, first order reversal curves, and Preisach modeling, J. Magn. Magn. Mater. 395 (2015) 361–375.
[47] P. Postolache, M. Cerchez, L. Stoleriu, A. Stancu, Experimental evaluation of the Preisach distribution for magnetic recording media, Ieee T Magn 39 (2003) 2531–2533.
[48] A.S. Samardak, A.V. Ognev, A.Y. Samardak, E.V. Stebliy, E.B. Modin, L.A. Chebotkevich, S.V. Komogortsev, A. Stancu, E. Panahi-Danaei, A. Fardi-Ilkhichy, F. Nasirpouri, Variation of magnetic anisotropy and temperature-dependent FORC probing of compositionally tuned Co-Ni alloy nanowires, J. Alloy. Comp. 732 (2018) 683–693.
[49] A. Stancu, C. Pike, L. Stoleriu, P. Postolache, D. Cimpoesu, Micromagnetic and Preisach analysis of the first order reversal curves (FORC) diagram, J. Appl. Phys. 93 (2003) 6620–6622.
[50] F. Preisach, , Über die magnetische Nachwirkung, Z. Phys. 94 (1935) 277–302.
[51] J.M.D. Coey, A.E. Berkowitz, L. Balcells, F.F. Putris, F.T. Parker, Magnetoresistance of magnetite, Appl. Phys. Lett. 72 (1998) 734–736.
[52] W. Eerenstein, T.T.M. Palstra, T. Hibma, S. Celotto, Origin of the increased resistivity in epitaxial Fe_3O_4 films, Phys. Rev. B 66 (2002) 201101.
[53] A.V. Ramos, J.B. Moussy, M.J. Guittet, A.M. Bataille, M. Gautier-Soyer, M. Viret, C. Gatel, P. Bayle-Guillemaud, E. Snoeck, Magnetotransport properties of Fe_3O_4 epitaxial thin films: thickness effects driven by antiphase boundaries, J. Appl. Phys. 100 (2006) 103902.
[54] P. Li, L.T. Zhang, W.B. Mi, E.Y. Jiang, H.L. Bai, Origin of the butterfly-shaped magnetoresistance in reactive sputtered epitaxial Fe_3O_4 films, J. Appl. Phys. 106 (2009), 033908.
[55] M. Ziese, R. Höhne, H.C. Semmelhack, H. Reckentin, N.H. Hong, P. Esquinazi, Mechanism of grain-boundary magnetoresistance in Fe_3O_4 films, Eur. Phys. J. B 28 (2002) 415–422.
[56] X. Liu, W. Mi, Q. Zhang, X. Zhang, Magnetoresistance of epitaxial and polycrystalline Fe_3O_4 films near Verwey transition, Appl. Phys. Lett. 113 (2018), 012401.
[57] J. Inoue, S. Maekawa, Theory of tunneling magnetoresistance in granular magnetic films, Phys. Rev. B 53 (1996) R11927–R11929.
[58] P.A. Miles, W.B. Westphal, A. Von Hippel, Dielectric spectroscopy of ferromagnetic semiconductors, Rev. Mod. Phys. 29 (1957) 279–307.